ARMA 16-177

Chemo-Mechanical Damage and Healing of Granular Salt: Micro-macro modeling

Xianda, Shen.[1], Zhu, C.[1], Arson, C.[1]

[1]*School of Civil and Environmental Engineering, Georgia Institute of Technology, Atlanta, Georgia*

ABSTRACT: A micro-macro chemo-mechanical model of damage and healing is proposed to predict the evolution of salt stiffness and deformation upon micro-crack propagation, opening, closure and rebonding, which is the result of pressure solution. We hypothesize that at a given grain contact, the surface area of the contact dictates which mechanism dominates the rate of healing. Based on thermodynamic equations of dissolution, diffusion and precipitation, we establish a formula for the critical contact area that marks the transition between diffusion-dominated kinetics and dissolution-precipitation-dominated kinetics. We relate the change of contact area to the change of solid volume in the Representative Elementary Volume, and we define net damage as the sum of the mechanical damage and the chemical porosity change. A continuum-based damage mechanics framework is used to deduce the change of salt stiffness with net damage. A stress path comprising a tensile loading, a compressive unloading, a creep–healing stage and a reloading is simulated. Stiffness degradation and residual strain development are observed with the evolution of damage under tensile loading. Unilateral effects of crack closure can be predicted by the model upon compression. Our micro-macro model also allows predicting the evolution of the probability distribution of contact areas upon healing, as well as the consequent decrease of net damage and recovery of stiffness. The proposed modeling framework is expected to shed light on coupled healing processes that govern microstructure changes and subsequent variations of deformation rate, stiffness and permeability in salt rock, and to allow the assessment of long-term behavior of geological storage facilities in salt.

1. INTRODUCTION

Salt rocks, a common geo-material with low gas permeability and favorable creep properties leading to potential fracture healing, are usually regarded as a favorable host for compressed air energy storage (CAES), radioactive waste repository, and gas storage.

During creep, crystal gliding mechanisms and grain sliding induce geometric incompatibilities, which build up stresses and intra-granular crack propagation. As grains rearrange, stresses at grain contacts can trigger dissolution, salt ion transport through fluid films, and re-precipitation at low-stress grain boundaries. This phenomenon, known as pressure-solution, can occur in the same conditions of pressure and temperature as grain boundary diffusion.

Quite a few pressure solution models for different geo-materials, such as calcite, halite and quartz, have been established, in which the controlling pressure solution mechanism is mostly influenced by the grains size, the number of grain contacts, effective stress and temperature. To study creep processes at the macroscopic scale, salt aggregates were made with various grain size distributions, immersed in a solution of saturated brine and tested in compression. Constitutive equations for creep rate and densification rate were derived (Raj, 1982). Compaction creep experiments on brine-saturated salt powder were conducted to model the influence of temperature, grain size and applied stress on creep deformation regimes (Spiers et al., 1990). Crack healing was studied at the crack scale, in single NaCl crystals. Experiments were conducted at a relative humidity of 75%, and healing was explained with a pressure solution model (Houben et al., 2013). Salt compaction as a result of NaCl pressure solution was also studied in (Brok et al., 1999). Analog experiments on crushed limestone and pure calcite's compaction behavior were conducted and the effects of applied stress, grain size, grain size distribution and various kinds of fluid were discussed in (Zhang and Spiers, 2005). The sealing and healing behavior of anhydrite gouge was discussed and detailed models for different pressure solution controlling mechanisms were developed to estimate the time scale on which such sealing and healing effects occur (Pluymakers and Spiers, 2014). Grain contact characteristics are the foundation for pressure solution analysis at the grain scale. Various hypotheses were formulated (e.g. Hickman and Evan, 1991; Noort and Spiers, 2009) to explain the phenomena that occur at the grain contacts, which were modeled as thin fluid films, island-channel networks, or thin films short-circuited by crack arrays.

In the long term, inelastic deformation in salt is generally influenced by dislocation, cross-slip, diffusive mass transfer (DMT) and recrystallization processes. Dislocation can result in stress concentration between grains and induce dilatant micro-cracking. DMT can both increases the creep strain and induces healing in salt (Voyiadjis et al. 2011). In order to study the damage and healing processes in halite, many mechanical models were established at both macro and micro scales. The effects of microscopic creep and cracking processes on salt deformation was discussed in (Chan et al. 2001), in which inelastic strain rate is assumed to be the sum of viscoplastic, damage and healing deformation rates. A mechanical anisotropic damage model under different stress and temperature conditions, considering a time-dependent healing behavior of halite was also proposed in (Xu and Arson, 2012). In (Zhu and Arson, 2014; Zhu and Arson, 2014), the effects of mechanical stress and temperature on crack opening and closure in rock are coupled within a thermodynamics-based model.

In this study, a coupled chemo-mechanical model is proposed to predict the effects of micro-crack propagation, opening, closure and chemical rebonding on halite stiffness, and to adapt the healing rate to microstructure evolution. Damage and healing micro-processes are presented in section 2. We establish formulas to calculate the change of contact area between grains during DMT and pressure solution healing processes. Section 3 presents a novel chemo-mechanical damage and healing model, in which macro-scale variables are coupled to microstructure descriptors. In Section 4, the model is used to simulate a stress path comprising a tensile loading, a compressive unloading, a creep–healing stage and a reloading.

2. MICROPROCESSES OF DAMAGE AND HEALING IN SALT

Dissolution, diffusion, and precipitation are the main processes that characterize pressure solution, and are key to understand chemo-mechanical damage and healing in salt. In order to study creep deformation rates, various models of pressure solution have been proposed for granular materials under compaction since the seminal work presented in (Rutter, 1976). Table 1 summarizes the representative models for each mechanism of pressure solution.

Table 1. Models of pressure solution

Pressure solution mechanism	Main governing equations	Reference
Solution	$\dot{\varepsilon}_s = \frac{A_s}{d} I_s \left[\exp\left(\frac{\sigma_e \Omega}{RT} \frac{Z}{F} \frac{q}{q-2\phi} \right) - 1 \right]$	Pluymakers and Spiers, 2014
	$\dot{\varepsilon} = K_s \frac{\sigma_e^n}{d f_s(\phi)}$	Zhang and Spiers, 2005
	$\dot{\varepsilon}_e = \frac{\sigma_e \Omega}{kT} \frac{k_1 \bar{c}}{d} \qquad \dot{\beta} = \frac{3\left(p_e - \frac{\gamma}{r}\Omega \right)}{kT} \frac{k_1' \bar{c}}{d}$	Raj,1982
precipitation	$\dot{\varepsilon}_p = \frac{A_p}{d} I_{pw} \left[\exp\left(\frac{\sigma_e \Omega}{RT} \frac{Z}{F} \frac{q}{q-2\phi} \right) - 1 \right] \frac{2\phi}{q-2\phi}$	Pluymakers and Spiers,2014
	$\dot{\varepsilon} = K_p \frac{\sigma_e^m}{d f_p(\phi)}$	Zhang and Spiers, 2005
diffusion	$\dot{\varepsilon}_d = \frac{2\pi A_c D C_s S Z}{\beta F d^3} \left[\exp\left(\frac{\sigma_e \Omega}{RT} \frac{Z}{F} \frac{q}{q-2\phi} \right) - 1 \right] \frac{2\phi}{q-2\phi}$	Pluymakers and Spiers, 2014
	$\dot{\varepsilon} = K_d \frac{\sigma_e}{d^3 f_d(\phi)}$	Zhang and Spiers, 2005
	$\dot{e} = \frac{32 \sigma_a V C_0 D_b S}{RT \rho d^3}$	Rutter, 1976
	$\dot{\varepsilon}_e = 2.3 \frac{\sigma_e \Omega}{\eta d^3} \bar{c} \alpha \; ; \; \alpha = \frac{xh}{b} \; ; \dot{\beta} = 6.9 \frac{\left(p_e - \frac{\gamma}{r} \right) \Omega}{\eta d^3} \bar{c} \alpha \; ; \quad \alpha = \frac{xh}{b}$	Raj,1982
	$\dot{\varepsilon} = 5 V_m \frac{Z^*}{T} \frac{\sigma}{d^3} \; ; \; Z^* = D_0 C_0 \exp(-\Delta H / RT) S \; ; \dot{\beta} = A V_m \frac{Z^*}{T} \frac{\sigma_e}{d^3 e_v^a} \; ; \; Z^* = D_0 C_0 \exp(-\Delta H / RT) S$	Spiers et al., 1990

Where $\dot{\varepsilon}$ is volumetric strain rate; $\dot{\beta}$ is the densification creep rate; K_s and K_p are incorporate temperature-dependent dissolution and precipitation rate coefficients; K_d is a temperature-dependent term incorporating the grain boundary diffusivity and width; σ_e is the applied effective stress; ϕ is the porosity; n and m are the exponential constants depending on dissolution and precipitation reaction orders; d is the grain size; A is a geometric factor depending on packing and deformation geometry; I is a rate constant; Ω is the molar volume of the solid phase; T is the absolute temperature; R is the gas constant; Z is the grain coordination number; F is a grain shape factor; q is a geometric term; D is the grain boundary diffusion coefficient; C_s is the local mean concentration of dissolved solid in grain boundary fluid; S is the mean fluid film thickness.

Based on pressure solution model presented by Pluymakers et al. (2014), we consider that the flat grain to grain contacts are penetrated by a thin fluid film. When an effective stress is applied to the solid skeleton of the salt sample, the drop $\Delta\tilde{\mu}_n$ in the normal component of solid chemical potential can be calculated as

$$\Delta\tilde{\mu}_n \approx \left(\tilde{\sigma}_n - P_f\right)\Omega \tag{1}$$

$$\Delta\tilde{\mu}_n \approx \frac{\sigma_n^e \Omega d_s}{a_c} \tag{2}$$

Where $\tilde{\sigma}_n$ is the local mean normal stress (MPa) acting on a given grain boundary element and Pf is the pore fluid pressure (MPa) acting on the free pore walls. Ω is the molar volume (2.7 × 10-5 m3 mol-1) for NaCl. d_s is the center-to-center grain spacing. a_c is the contact area.

Due to the compression-induced chemical potential difference between grain contact and pore wall surface, material dissolves at grain contact, diffuses along the grain boundary and precipitates at the pore wall surface, showed in Fig.1.

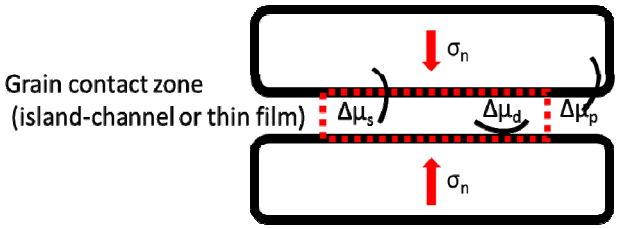

Fig. 1. Pressure solution mechanism

Since pressure solution is a sequential process, the chemical potential drop from source and sink is the sum of each chemical drop related to solution, precipitation and diffusion. Considering steady-state mass transfer from grain contacts to pore walls, the corresponding equation is:

$$\Delta\tilde{\mu}_n = \Delta\tilde{\mu}_s + \Delta\tilde{\mu}_d + \Delta\tilde{\mu}_p \tag{3}$$

For the solution mechanism,

$$\Delta\tilde{\mu}_n = RT\ln\left(1+\frac{\Delta\tilde{C}}{\tilde{C}_f}\right) \tag{4}$$

$$V_{dis} = I_s\left(\exp\left(\frac{\sigma_n^e \Omega d_s^2}{RTa_c}-1\right)\right) \tag{5}$$

$\Delta\tilde{C}$ is the absolute enhanced solubility at grain contact sites. $\tilde{C}_f$ is the concentration of the dissolved solid in the grain boundary fluid. V_{dis} is the velocity of the dissolving interface due to dissolution. If $\sigma_n^e \Omega d_s^2 / RTa_c$ is small enough, V_{dis} can be simplified as

$$V_{dis} = I_s \frac{\sigma_n^e \Omega d_s^2}{RTa_c} \tag{6}$$

The shortening rate of salt particle diameters can be obtained using $-\dot{d}_s/2 = V_{dis}$. After integration, we can get the time evolution law of the contact length between two particles, as follows:

$$-\frac{\dot{d}_s}{2} = I_s \frac{\sigma_n^e \Omega d_s^2}{RTa_c} \tag{7}$$

$$\frac{\pi RT}{8\sigma_n^e I_s}\left(\frac{2d_p^2 - x^2}{\sqrt{2d_p^2 - x^2}} - \frac{2d_p^2 - x_0^2}{\sqrt{2d_p^2 - x_0^2}}\right) = t \tag{8}$$

$$a_c = \pi x^2 / 4 \tag{9}$$

Where d_p is the diameter of grains and x is the contact length. We assume $V_{pre} = \alpha V_{dis}$ and $I_p = \alpha I_s$. Like for the dissolution mechanism, the precipitation mechanism is governed by the following equations:

$$\Delta\mu_n = \Delta\mu_p \tag{10}$$

$$V_{pre} = I_p \frac{\sigma_n^e \Omega d_s^2}{RTa_c} \tag{11}$$

If $\sigma_n^e \Omega d_s^2 / RTa_c$ is small enough, V_{pre} can be simplified as:

$$-\frac{\dot{d}_s}{2} = -I_p \frac{\sigma_n^e \Omega d_s^2}{RTa_c} \tag{12}$$

$$\frac{\pi RT}{8\sigma_n^e I_p}\left(-\frac{2d_p^2 - x^2}{\sqrt{2d_p^2 - x^2}} + \frac{2d_p^2 - x_0^2}{\sqrt{2d_p^2 - x_0^2}}\right) = t \tag{13}$$

For the diffusion mechanism, we have:

$$\Delta\mu_n = \Delta\mu_d \tag{14}$$

If $\sigma_n^e \Omega d_s^2 / RTa_c$ is small enough, V_{dif} can be simplified as:

$$V_{dif} = \frac{2\pi DC_0 S\Omega}{\beta a_c} \frac{\sigma_n^e \Omega d_s^2}{RTa_c} \tag{15}$$

$$-\frac{\dot{d}_s}{2} = \frac{2\pi DC_0 S\Omega}{\beta a_c} \frac{\sigma_n^e \Omega d_s^2}{RTa_c} \tag{16}$$

$$A\begin{pmatrix} d_p^4 \ln\left(\left(d_p^2 - x^2\right)^{\frac{1}{2}}\right) - d_p^2\left(d_p^2 - x^2\right) + \frac{1}{4}\left(d_p^2 - x^2\right)^2 \\ -d_p^4 \ln\left(\left(d_p^2 - x_0^2\right)^{\frac{1}{2}}\right) + d_p^2\left(d_p^2 - x_0^2\right) - \frac{1}{4}\left(d_p^2 - x_0^2\right)^2 \end{pmatrix} = t \tag{17}$$

$$A = \frac{\beta RT\pi}{64 DC_0 S\Omega^2 \sigma_n^e} \tag{18}$$

Generally, the contact area between halite grains is not uniform. We found our micro-macro model on the coupling between the evolution of the macroscopic damage and healing variables with that of the contact area probability density function. We compare the values of V_{dis}, V_{pre}, V_{dif} in order to find the dominating mechanism of pressure solution for a given contact area. We note that V_{dis} / V_{pre} does not depend on the contact area. The diffusion mechanism controls the speed of material diffusion along the grain boundary. If V_{dif} is larger than V_{dis} or V_{pre}, diffusion will be the dominating mechanism. As α is generally less than 1, V_{dis} is larger than V_{pre}. We define the critical contact area a_c^* as the threshold between diffusion–dominated deformation and dissolution-precipitation dominated deformation. From the ratio between V_{diff} and V_{pre}, we get:

$$a_c^* = \frac{2\pi DC_0 S\Omega}{I_p} \tag{19}$$

If $a_c < a_c^*$, $\min(V_{dis}, V_{pre}) < V_{dif}$, i.e. diffusion dominates. Otherwise, dissolution-precipitation dominates (Fig.2).

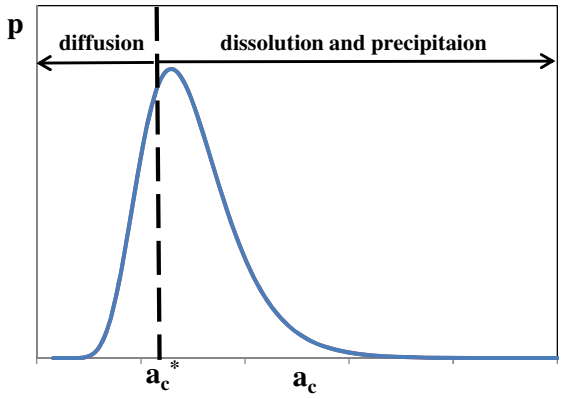

Fig. 2. Definition of the critical contact area

For each dominating mechanism, the expression of the increment of contact area over a small time increment can be obtained, as follows:

$$\delta a_c^{dis,pre} = \delta a_c^{dis} + \delta a_c^{pre} = (I_s - I_p) \frac{\pi \sigma_n^e \Omega \left(d_p^2 - 4a_c/\pi\right)^{3/2}}{RTa_c} \delta t \tag{20}$$

$$\delta a_c^{dif} = \frac{2\pi^2 DC_0 S\Omega^2 \left(d_p^2 - 4a_c/\pi\right)^{3/2}}{\beta RTa_c^2} \delta t \tag{21}$$

The average contact area over the entire domain of study (Representative Elementary Volume) is determined as

$$a_c(t) = \int_{\min}^{thre} p(x) a_{cdif}(t) dx + \int_{thre}^{\max} p(x) a_{dis,pre}(t) dx \tag{22}$$

3. MICRO-MACRO CHEMO-MECHANICAL MODEL OF DAMAGE AND HEALING

3.1. Continuum-based chemo-mechanical model of damage and healing

The model established in is this paper couples chemical and mechanical effects, to analyze the influence of micro-cracks' opening, closure and healing on salt rock's deformation and stiffness. The strain ε is the sum of the purely elastic strain ε^{el}, the elastic strain induced by the degradation of elastic moduli with damage ε^{ed}, and the irreversible strain due to cracks ε^{id} (Fig.3; Zhu and Arson, 2015).

$$\varepsilon = \varepsilon^{el} + \varepsilon^{d} = \varepsilon^{el} + \varepsilon^{ed} + \varepsilon^{id} \tag{23}$$

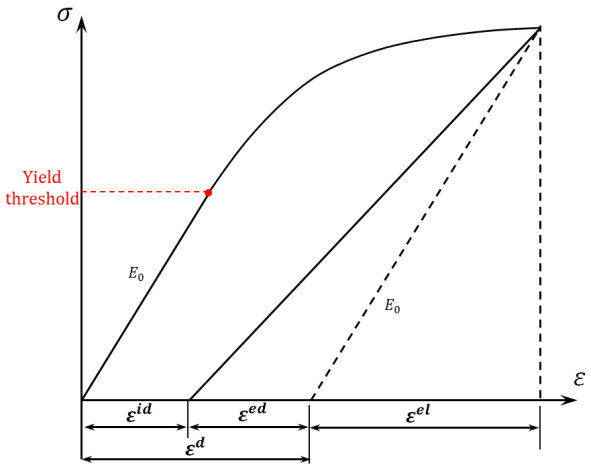

Fig. 3. Strain decomposition for a typical loading and unloading cycle

Rock without damage is assumed to have a linear thermo-elastic behavior, and the damage variable Ω used in the model is a second-order tensor. The free energy of the rock solid skeleton Ψ_s is decomposed into three parts: the purely elastic-thermo energy Ψ_s^{ET} and the potential energy that can be dissipated by damage $\Psi_s^{\Omega T}$ and the potential energy that can be dissipated by

healing, Ψ_s^{HT}. For illustrative purposes, we present the thermodynamics equations of the model with no healing:

$$\psi_s = \psi_s^{ET} + \psi_s^{\Omega T} \tag{24}$$

$$\psi_s^{ET} = \frac{1}{2}\varepsilon^{el} : \mathbb{C}_0 : \varepsilon^{el} - \frac{C_0\tau^2}{2\tau_0} - \tau K_0 : \varepsilon^{el} \tag{25}$$

$$\psi_s^{\Omega T} = \frac{1}{2}\varepsilon^{d} : \mathbb{C}(\Omega) : \varepsilon^{d} - \frac{C(\Omega)\tau^2}{2\tau_0} - \tau K(\Omega) : \varepsilon^{d} \tag{26}$$

$$K(\Omega) = k(\Omega)\alpha_T\delta \tag{28}$$

Where Ω is damage tensor, C is the heat capacity, τ is the temperature variation, k is the bulk modulus, and α_T is the thermal dilation coefficient. According to Halm & Dragon's model (Dragon et al., 1998), the expression of deformation energy of salt rock is given:

$$\begin{aligned}&\frac{1}{2}\varepsilon^{d} : \mathbb{C}(\Omega) : \varepsilon^{d} = \frac{1}{2}\lambda(tr\varepsilon^{d})^2 + \mu tr(\varepsilon^{d}\cdot\varepsilon^{d}) \\ &+\alpha tr\varepsilon^{d} tr(\varepsilon^{d}\cdot\Omega) + 2\beta tr(\varepsilon^{d}\cdot\varepsilon^{d}\cdot\Omega)\end{aligned} \tag{29}$$

Where α and β are damage parameters. λ and μ are Lamé coefficients.

The stress and damage driving force tensors Y are obtained by thermodynamic conjugation

$$\sigma = \frac{\partial\Psi_s}{\partial\varepsilon^{el}} = \frac{\partial\Psi_s^{ET}}{\partial\varepsilon^{el}} \tag{30}$$

$$Y = \frac{\partial\Psi_s}{\partial\Omega} = \frac{\partial\Psi_s^{\Omega T}}{\partial\Omega} \tag{31}$$

A linear damage function is used for the propagation criterion, to simulate the hardening phenomenon. Assuming that the damage flow rule is associative, the propagation criterion is used as the damage potential:

$$f_d(Y_d,\Omega) = \sqrt{\frac{1}{2}Y_d : Y_d} - \left[a_0 + a_1 tr(\Omega)\right] \tag{32}$$

$$d\Omega = d\lambda_d \frac{\partial f_d(Y_d,\Omega)}{\partial Y_d} \tag{33}$$

Where a_0 is the initial damage threshold and a_1 is the hardening rate parameter. $d\lambda_d$ is the damage multiplier.

Due to the effect pressure solution, the area of contact between grains increases over time. Driven by dissolution, precipitation and diffusion, the volume of voids in stressed halite rocks decreases, which results in porosity changes. Cracks closure and rebonding may lead to salt mechanical recovery, which can be regarded as healing. In this paper, the chemo-mechanical effect is assumed to relate to the change of porosity. The net damage A is regarded as the sum of thermo-mechanical damage and chemo-mechanical damage, and its expression is given by:

$$A = \Omega + \Delta\phi_c \tag{34}$$

3.2. *Micro-macro coupling*

In order to link microstructure descriptors and macroscopic variables of damage and healing, a model is proposed to relate the evolution of grain contact area to the change of chemical porosity involved in the definition of net damage (Eq.34). We assume that grains are initially spherical, and that upon pressure solution, spherical caps at the grain contacts are dissolved. When the contact area increases, more salt is dissolved, and the volume of solid salt deceases. Fig.4 illustrates the geometric relationship between the contact area and the volume of dissolved salt.

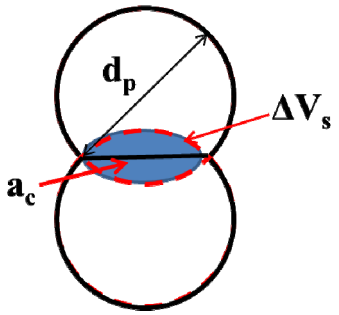

Fig.4. Relationship between contact area and volume of dissolved salt

The expression of δV_s is obtained geometrically, as:

$$\delta V_s = \left(\begin{array}{l} \dfrac{4\left(d_p - \sqrt{d_p^2 - 4a_c/\pi}\right)\left(2d_p + \sqrt{d_p^2 - 4a_c/\pi}\right)}{6\sqrt{d_p^2 - 4a_c/\pi}} \\ -\dfrac{2\left(d_p - \sqrt{d_p^2 - 4a_c/\pi}\right)^2}{6\sqrt{d_p^2 - 4a_c/\pi}} \end{array} \right) \delta a_c \tag{35}$$

During pressure solution-driven healing processes, the change of chemical porosity is calculated as:

$$\delta V_s = -\delta V_v \tag{36}$$

$$\Delta\phi_c = \frac{\delta V_v}{V_{REV}} = -\frac{\delta V_s}{V_{REV}} \tag{37}$$

Note that in (Eq.37) we assumed that V_{REV} is constant. In our resolution algorithm, V_{REV} is actually constant over e very time step only. At each time step, the change of che mical porosity is updated with the evolution of the conta ct areas, which induces stiffness changes under constant stress, and therefore deformation and changes of V_{REV}.

4. SIMULATION OF LOADING/ UNLOADING CYCLES WITH A HEALING STAGE

4.1. *Material parameters and stress path*

The chemo-mechanical damage and healing model presented in Section 3 was used to simulate a stress path comprising a tensile loading, a compressive unloading, a

creep–healing stage and a reloading. The material parameters (Table 2) are chosen according to the recommendations made in (Zhu and Arson, 2014) and (Houben et al., 2013). We assume the initial average diameter of contact area is 0.3 of the grain diameter.

Table 2. Model parameters used in the simulations

λ(Pa)	μ(Pa)	a(Pa)	b(Pa)
2.63×10^{10}	1.75×10^{10}	1.9×10^{9}	-2.04×10^{10}
C_0(Pa)	C_1(Pa)	g(Pa)	B(Pa)
1000	5.5×10^{5}	1.1×10^{8}	0
d_p(m)	Ω (m^3/mol)	C(mol/m^3)	T(K)
0.0002	2.7×10^{-5}	0.1675	296
DS(m^3/s)	I_s(m/s)	I_p(m/s)	m_{ac}(mm^2)
1.3×10^{-14}	1.0×10^{-9}	2×10^{-10}	2.89×10^{-9}
σ_{ac} (mm^2)			
1.0			

Five loading phases are considered (Fig. 5):

(M1) Axial tension. The sample is loaded by decreasing the axial strain (direction 1) at a constant strain rate, until the axial strain reaches a minimum axial strain of -0.0006). The lateral stresses do not change throughout this phase.

(M2) Axial compression. The sample is loaded by increasing the axial strain (direction 1) at a constant strain rate, until the axial strain reaches a maximum axial strain of 0.0006). The lateral stresses do not change throughout this phase.

(H) Healing (creep stage). Axial compressive stress is fixed at this stage. The healing of salt rocks occurs due to pressure solution. For grain contact areas below the critical contact area a_c*, the healing rate is that of diffusion. This stage will last for 100,000 seconds.

(M3) Axial tension. The sample is loaded by decreasing the axial strain (direction 1) at a constant strain rate, until the axial strain reaches a minimum axial strain of -0.00099). The lateral stresses do not change throughout this phase.

(M4) Axial compression. The sample is loaded by increasing the axial strain (direction 1) at a constant strain rate, until the axial strain reaches a maximum axial strain of 0.00051). The lateral stresses do not change throughout this phase.

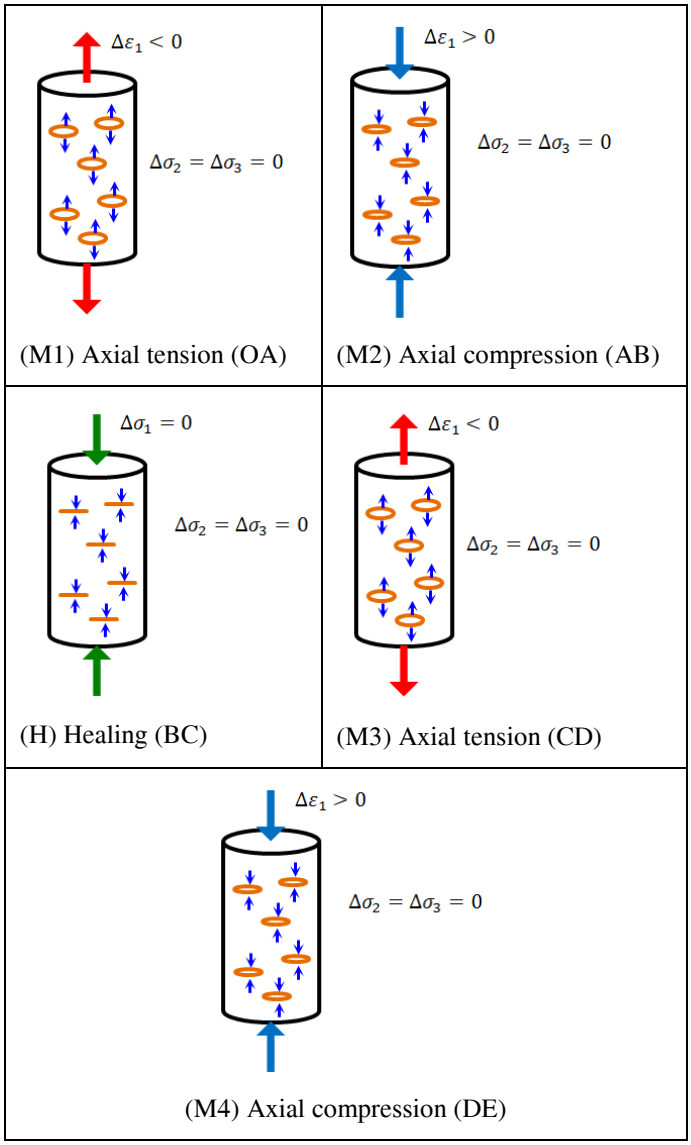

Fig. 5. Loading path for the simulation of damage and healing

4.2. *Results and discussion*

Stress/strain curves are presented in Fig. 6. Rock tensile strength is relatively low, so that damage starts to develop quickly during phase (M1). Cracks occur and open, and stiffness degradation is observed (OA). After the strain of sample reaches -0.0006, the sample is unloaded, elastically, first in tension with a damaged stiffness (AA_1) and then in compression, with the reference stiffness recovered by unilateral effects of crack closure (A_1B). At the end of the compression phase (M2), strain reaches 0.0006. Then, the salt sample starts to heal. During this healing stage (BC) of 100,000 seconds, cracks rebond. As a result, the net damage variable decreases and the stiffness increases. During the second tension phase (CD), the slope of the stress/strain curve is larger than during the compression phase (AB), due to healing effects. However, after a critical tension stress, damage starts to develop again and more cracks are opened. Finally, the sample is unloaded and compressed again (DE). The same unilateral effects are

observed when cracks are closed (i.e., slope DD_1 is smaller than slope D_1E).

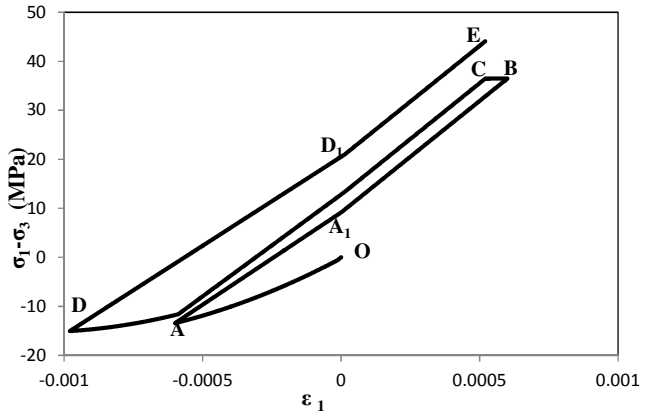

Fig. 6. Deviatoric stress versus axial deformation

Fig. 7 shows the development of damage (Ω_1) and net damage (A_I). When tensile loading is applied, both Ω_1 and A_I increase. Vertical damage (Ω_1) does not develop during the unloading and compression stage. The net damage A_I decreases during healing (BC). After this stage, many cracks are assumed to be healed.

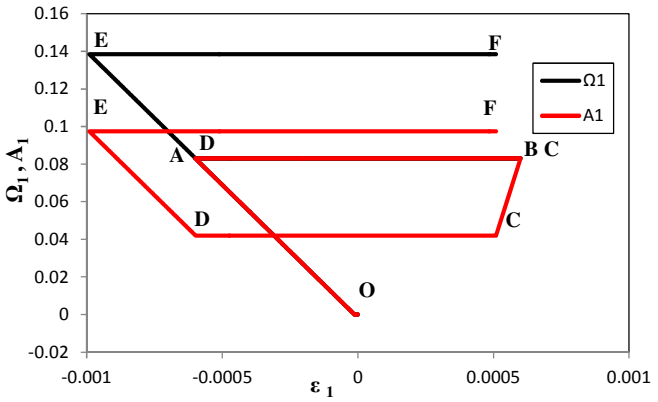

Fig. 7. Evolution of damage and net damage

In the absence of reference data, we assume that the contact area between salt grains is lognormal distributed. The initial mean of contact area is 2.89×10^{-9} mm^2. The threshold contact area is $a_c^* = 2.73\times10^{-9}$ mm^2. If the contact area is less than 2.73×10^{-9} mm^2, healing is dominated by diffusion. While, if contact area is larger than 2.73×10^{-9} mm^2, the healing process is dissolution-precipitation dominated. Fig. 8 presents the evolution of the probability density function (PDF) of contact area during the healing process. For extended periods of healing time, contact areas increase and cracks close and heal. The peak of the PDF curve is 3.23×10^{-9} mm^2 after healing for 10,000 seconds, and 5.62×10^{-9} mm^2 after 50,000 seconds. The peak reaches 7.42×10^{-9} mm^2 after 100,000 seconds. According to Fig.8, healing at the sample scale is totally dissolution-precipitation dominated for healing periods over 50,000 seconds. Examining the shape of the PDF curve over time, it can be noted that the PDF curves become sharper with the increase of time, which means that the distribution of contact areas becomes more uniform, and the increasing speed of larger contact area is slower than small one. This phenomenon can also be verified by comparing the increase of PDF peak contact area with time. The rate of contact area increase is high at the beginning of the healing, and then it slows down.

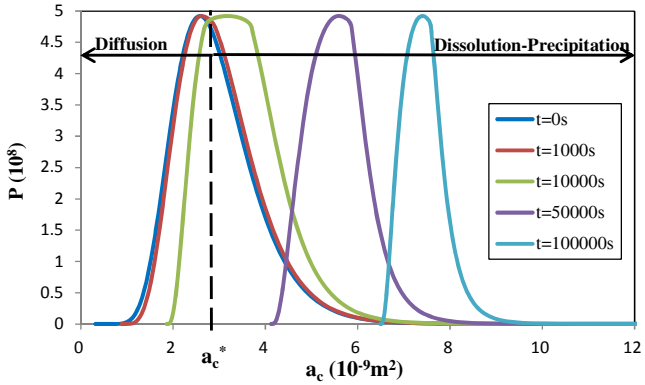

Fig. 8. PDF of contact area during healing process

Fig. 9 shows the evolution of net damage A_I with the healing time. Before the healing phase, the net damage is equal to the mechanical damage. Then, as cracks start to heal, the net damage decreases. The curve presented in Fig. 9 is not a straight line. As healing proceeds in the sample, the area of the contacts between grains increases, so that healing becomes progressively dominated by dissolution-precipitation. This transition from mixed diffusion healing and dissolution-precipitation healing towards dissolution-precipitation only results in an increase of the rate of recovery. The slope of the curve becomes slightly steeper over time, which is in agreement with the model assumptions.

CONCLUSION

Damage and healing plays a significant role in the mechanical behavior of salt rocks. The model proposed in this paper takes both damage and healing into consideration. Mechanical damage represents the propagation and opening of micro-cracks that contribute to material softening. Crack rebonding is the result of pressure solution, which occurs at the rate of the dominating micro-mechanism, i.e. dissolution, diffusion or precipitation. In our model, we hypothesize that at a given grain contact, the surface area of the contact dictates which mechanism dominates the rate of healing. Based on thermodynamic equations of dissolution, diffusion and precipitation, we establish a formula for the critical contact area that marks the transition between diffusion-dominated kinetics and dissolution-precipitation-dominated kinetics. We relate the change

of contact area to the change of solid volume in the Representative Elementary Volume, and we define net damage as the sum of the mechanical damage and the chemical porosity change. A continuum-based damage mechanics framework is used to deduce the change of salt stiffness with net damage. Loading and unloading cycles comprising a creep healing phase were simulated. Stiffness degradation and residual strain development are observed with the evolution of damage under tensile loading. Unilateral effects of crack closure can be predicted by the model upon compression. Our micro-macro model also allows predicting the evolution of the probability distribution of contact areas upon healing, as well as the consequent decrease of net damage and recovery of stiffness. Our next task is to calibrate the model against actual experimental results and to extend the formulation to chemo-hydro-mechanical couplings in order to study the impact of healing not only on mechanical salt properties, but also salt permeability. In addition to its relevance to geological energy storage in halite, including compressed air energy storage (CAES), radioactive waste repository, and gas storage, the proposed modeling framework is expected to improve predictions of deformation and stiffness upon healing in other materials such as quartz, calcite, concrete and cement.

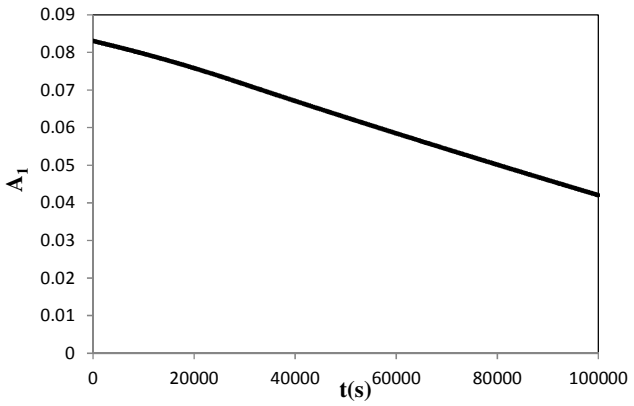

Fig. 9. Evolution of net damage with time

ACKNOWLEDGEMENTS

Financial support for this research was provided by the National Science Foundation (Grant No. CMMI-1362004/1361996).

REFERENCES

1. Brok, B., Zahid, M., Passchier, C.W, 1999. Pressure solution compaction of sodium chlorate and implications for pressure solution in NaCl. *Tectonophysics*. 307 (1999) 297–312

2. Chan, K.S., S.R. Bodner, and D.E. Munson., 2001. Permeability of WIPP Salt during Damage Evolution and Healing. *International Journal of Damage Mechanics*, 10:347-375.

3. Dragon A, D. Halm, T. De´soyer, 2000 Anisotropic damage in quasi-brittle solids: modelling, computational issues and applications. *Comput Methods Appl Mech Eng* 183(3):331–352

4. Hickman, S. J. and B. Evan, 1991 Experimental pressure solution in halite: the effect of grain/interphase boundary structure. *Journal of the Geological Society.* Vol. 148, 1991, pp. 549-560

5. Houben, M., A. ten Hove, C. Peach, and C. Spiers, 2013. Crack healing in rocksalt via diffusion in adsorbed aqueous films: Microphysical modelling versus experiments. *Physics and Chemistry of the Earth*, Parts A/B/C 64, 95-104.

6. Xu, H. and C.Arson, 2012. Stiffness and Deformation of Salt Rock Subject to Anisotropic Damage and Temperature-Dependent Healing. *The proceeding of 46th U.S. Rock Mechanics/Geomechanics Symposium*. ARMA 12-316.

7. Noort, R. and C. J. Spiers, 2009. Kinetic effects of microscale plasticity at grain boundaries during pressure solution. *Journal of Geophysical Research. Res*., 114, B03206

8. Pluymakers, A. and C. J. Spiers, 2014. Compaction creep of simulated anhydrite fault gouge by pressure solution: theory vs. experiments and implications for fault sealing. Geological Society, London, Special Publications 409, SP409-6.

9. Raj, R., 1982. Creep in polycrystalline aggregates by matter transport through aliquid phase. *J. Geophys. Res*. 87 (B6), 4731–4739.

10. Rutter, E., 1983. Pressure solution in nature, theory and experiment. *Journal of the Geological Society* 140 (5), 725-740.

11. Spiers, C., P. Schutjens, R. Brzesowsky, C. Peach, J. Liezenberg, and H. Zwart, 1990. Experimental determination of constitutive parameters governing creep of rocksalt by pressure solution. *Geological Society,* London, Special Publications 54 (1), 215-227.

12. Voyiadjis G.Z., A. Shojaei, and G. Li, 2011. A thermodynamic consistent damage and healing model for self healing materials. *Int J Plast* 27(7):1025–1044

13. Zhang, X. and C. Spiers, 2005. Compaction of granular calcite by pressure solution at room temperature and erects of pore fluid chemistry. *International Journal of Rock Mechanics and Mining Science*s 42 (7), 950-960.

14. Zhu, C., and C. Arson, 2015. A Model of Damage and Healing Coupling Halite Thermomechanical Behavior to Microstructure Evolution. *Geotech Geol Eng* (2015) 33:389–410

15. Zhu C, and C Arson, 2014. A thermo-mechanical damage model for rock stiffness during anisotropic crack opening and closure. *Acta Geotech* pp. doi:10.1007/s11,440-013-0281-0